

# DME/TACAN interference mitigation for GNSS: algorithms and flight test results

Grace Xingxin Gao · Liang Heng ·  
Achim Hornbostel · Holmer Denks ·  
Michael Meurer · Todd Walter · Per Enge

Received: 6 February 2012 / Accepted: 8 November 2012 / Published online: 29 November 2012  
© Springer-Verlag Berlin Heidelberg 2012

**Abstract** The Galileo E5a/E5b signals and the Global Positioning System (GPS) L5 signal lie within the aeronautical radionavigation services (ARNS) band. They suffer interference from the services in this frequency band, in particular, pulsed signals from distance measuring equipment (DME) and tactical air navigation (TACAN) systems. To maintain system accuracy and integrity, interference mitigation is beneficial and necessary. We first present the real DME/TACAN environment at Stanford, CA as an example to illustrate the need for mitigating DME/TACAN interference. We then propose a time and frequency joint mitigation algorithm—Hybrid Blanking and its simplified version, frequency domain adaptive filtering (FDAF) for hardware implementation. Finally, a flight measurements

campaign was performed over a European DME/TACAN hotspot near Frankfurt, Germany, to record a worst-case DME interference environment. Recorded data from the flight tests mixed with injected GNSS signals verify the effectiveness of the proposed mitigation algorithm.

**Keywords** GPS · Galileo · DME · Interference mitigation

## Introduction

Unlike their L1 and E6 counterparts, Galileo/GPS E5a and L5 signals at 1,176.45 MHz and Galileo E5b signals at 1,207.14 MHz are exposed to a unique electromagnetic environment created by existing aeronautical system pulsed emitters, especially distance measuring equipment (DME) and tactical air navigation (TACAN) systems. DME provides distance measurement between aircraft and a ground station by timing the propagation delay of the wireless radio signals. TACAN additionally provides azimuth information and is a military system. These navigation systems consist of an airborne interrogator and a ground-based transponder. DME and TACAN operate in the frequency span between 960 and 1,215 MHz in an aeronautical radionavigation services (ARNS) band. DME transponders transmit in the frequency band from 962 to 1,150 MHz and receive on a frequency that is offset from the transmit frequency by 63 MHz (Kim and Grabowski 2003). The ARNS frequency allocation chart in Fig. 1 illustrates its overlap with the E5 band. DME signal is composed of pulse pairs with an inter-pulse interval of 12  $\mu$ s (Bastide et al. 2004; RTCA 2004).

The DME/TACAN interference degrades the signal-to-interference plus noise ratio (SINR) (Gao 2007; Kayton and Fried 1997) potentially causes the tracking loops of

---

G. X. Gao (✉)  
Department of Aerospace Engineering, University of Illinois  
at Urbana-Champaign, Urbana-Champaign, IL, USA  
e-mail: gracegao@illinois.edu

G. X. Gao · L. Heng  
University of Illinois at Urbana-Champaign,  
Urbana-Champaign, IL, USA

A. Hornbostel  
Institute of Communications and Navigation,  
German Aerospace Center (DLR), Cologne, Germany

H. Denks  
Galileo Control Centre, Wessling, Germany

M. Meurer  
Department of Navigation of the German Aerospace Center  
(DLR), Institute for Communications and Navigation,  
Cologne, Germany

T. Walter · P. Enge  
Department of Aeronautics and Astronautics,  
Stanford University, Stanford, CA, USA

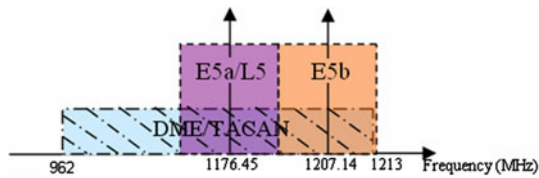


Fig. 1 ARNS frequency allocation

receivers to fail to converge if no mitigation method is applied.

There has been research conducted on mitigating DME/TACAN interference based on hardware simulations (Denks et al. 2008, 2009). We not only propose new algorithms, but also use live data collected from in situ flight tests injected with generated GNSS signals and real-world environments to verify our algorithms using our software receiver.

The “Problem statement” section describes the DME/TACAN pulse structure. The DME/TACAN interference environment at Stanford, CA, USA is illustrated as an example to show the sparsity of time and frequency characteristics. “Mitigation Algorithms” section focuses on the algorithms. A time–frequency hybrid blanking algorithms are proposed to mitigate the pulsed interference. This has advantage over existing single domain methods, such as time domain pulse blanking and frequency domain notch filtering. Considering the complexity for hardware implementation, a simplified algorithm, frequency domain adaptive filtering (FDAF), is also proposed in this section. “On-Flight Data Collection at European DME Hotspot” section presents the on-flight DME/TACAN data collection, including the test aircraft, the mounted antenna, etc. “Flight and ground test results” section shows the effectiveness of our proposed DME/TACAN algorithms compared to current existing algorithms in two situations. One is the worst-case situation of GNSS signals injected with on-flight data collected at the DME hotspot in Europe. The other one is the quieter situation of the live data collected on the roof of our Stanford GPS Laboratory. “Conclusion” section concludes the paper.

**Problem statement**

**DME/TACAN signal structure overview**

In the DME system, aircraft interrogators transmit pulses paired 12 μs apart, with each pulse lasting 3.5 μs. The peak pulse power varies from 50 W to 2 kW. Paired pulses are used in order to reduce interference from other systems (Kayton and Fried 1997). The pulse pair repetition rate is bonded from 800 to 4,800 pulse pairs per second based on specification. Practically, the maximum rate is 2,700 pulse

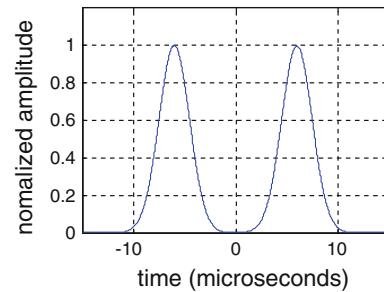


Fig. 2 A simulated DME pulse pair

pairs per second. Typical values are in the range from 1,200 to 1,500 pulse pairs per second (EUROCAE 1987).

Each pulse can be modeled as a Gaussian function. A pulse pair has the following expression (Kayton and Fried 1997), which is illustrated in Fig. 2,

$$s_{\text{pulse-pair}}(t) = e^{-\frac{\alpha}{2}t^2} + e^{-\frac{\alpha}{2}(t-\Delta t)^2}$$

where  $\alpha = 4.5 \times 10^{11} \text{ s}^{-2}$  and  $\Delta t = 12 \times 10^{-6}$ .

The constant  $\alpha$  determines the pulse width, while  $\Delta t$  is the inter-pulse interval.

TACAN transponders transmit DME pulse pairs plus bearing reference pulses. A 15 Hz so-called north reference pulse code is emitted once per revolution, coincident with the maximum of the antenna pattern pointing east. This comprises 24 pulses, the spacing between pulses being alternately 12 and 18 μs. Eight times per revolution, the 135 Hz reference pulse group of 12 pulses spaced 12 μs apart is emitted. (The ninth group coincides with the north pulse and is intentionally omitted.) The reference pulse groups have higher priority than normal constant-duty-cycle pulses. The overall transmitted pulse envelope is shown in Fig. 3. The TACAN signals are amplitude modulated by a rotating antenna, thus reducing the effective sensitivity of the TACAN beacon about 3 dB below that of an ordinary DME beacon (Kayton and Fried 1997).

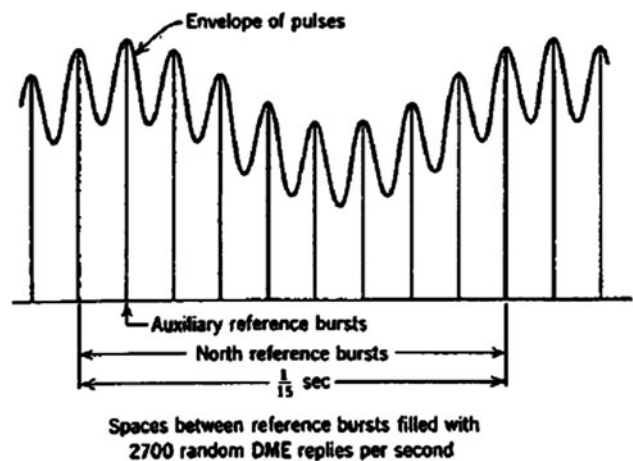


Fig. 3 Transmitted TACAN signal (Kayton and Fried 1997)

A DME only transponder transmits DME pulses with no amplitude modulation. A DME/TACAN transponder transmits DME pulses with amplitude modulation plus bearing reference pulses. For a DME receiver receiving signals from a DME/TACAN transponder, it ignores the amplitude modulation, and only processes the pulses.

**Real DME/TACAN signals: a close look at the time frequency properties**

In this subsection, we use real DME/TACAN signals to illustrate their unique properties—sparsity in both time and frequency domain.

The signal is captured by the Stanford GNSS monitor system (SGMS). A 1.8 m parabolic dish antenna is set up on the roof of a four-story building at Stanford, CA, USA. The main lobe of the antenna is pointing to a Galileo In-Orbit Validation Element (GIOVE)-A satellite. The antenna side lobes capture the DME/TACAN signals.

#### *Frequency domain sparsity*

Figure 4a, b show the power spectral density of the E5a and E5b frequency bands, respectively. There are spikes in the frequency domain, corresponding to nearby DME/TACAN transponders, namely SJC, SFO, Sausalito, OAK, and Moffet, as marked. The height of the spikes represents the received power of corresponding DME/TACAN signals. The received power is a function of the distance from the airports to the observing location, the elevation of the airports, and the transmitted power level. Table 1 shows the longitude, latitude, site elevation, antenna height, and transmitter power of the DME/TACAN beacons around Stanford University. Figure 5 shows the map of the all these DME transponders with respect to Stanford. The woodside spike is the highest in the spectrum due to the beacon's proximity and its high elevation.

#### *Time domain sparsity*

The received E5a signal in the time domain is illustrated in Fig. 6. The signal is amplitude modulated with envelope period of 66.67 ms, or equivalently at 15 Hz. This is generated by a parasitic element rotating around the antenna at 900 rpm. On top of the 15 Hz modulation, there is another 135 Hz sinusoidal modulation generated by nine other parasitic elements, also rotating at 900 rpm.

If we zoom in, we can see DME pulse pairs with a Gaussian shape as shown in Fig. 7. It verifies the pulse width of 3.5  $\mu$ s and inter-pulse interval of 12  $\mu$ s as described in the “DME/TACAN signal structure” section.

The DME/TACAN signals are sparse not only in the frequency domain, but also in the time domain. Both time

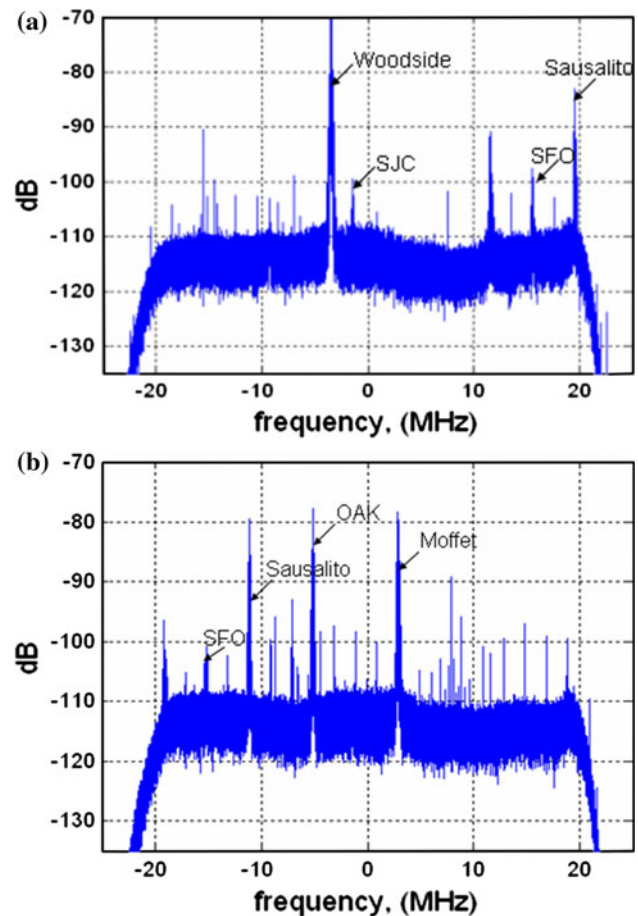


**Fig. 4** a E5a power spectral density, b E5b power spectral density

and frequency amplitude of the DME/TACAN signals well exceed the noise floor, while the GNSS signals (in this case the GIOVE-A E5 signals) are buried under noise. Therefore, it is important to mitigate the DME/TACAN interference for GNSS receivers. In the next section, we will propose algorithms for DME/TACAN interference mitigation based on this unique property of time and frequency sparsity.

### **Mitigation algorithms**

Previous studies have addressed DME/TACAN interference. These can be categorized into two groups—time domain approach and frequency domain approach.

Existing time domain algorithm: pulse blanking

Pulse blanking has been discussed in Kim and Grabowski (2003) and Bastide et al. (2004) as the time domain mitigation technique. It blanks the signal portions if the norm of their amplitude exceeds a certain threshold level.

**Table 1** DME/TACAN beacons near Stanford, CA, USA

Airport	Longitude	Latitude	Site elevation (ft)	Antenna height (ft)	Transmitter power (W)
Woodside	37.39278	−122.28194	2,215	16	1,173
Moffet	37.43222	−122.05694	4	N/A	1,210
SFO	37.61944	−122.37389	13	26	1,192
SJC	37.37472	−121.94472	56	33	1,175
OAK	37.72583	−122.22333	10	N/A	1,202
Sausalito	37.85528	−122.5225	1,040	N/A	1,196



**Fig. 5** Map of DME transmitters near Stanford University

Figures 8 and 9 show the time domain E5a signal before and after pulse blanking. Figure 10 shows the power spectrum. In this example, pulse blanking mitigates 22 dB of DME/TACAN interference, reducing the spikes from −70 to −92 dB. However, smaller spikes still exist at 17 dB above the noise floor.

Pulse blanking is effective and simple to implement but is not thorough due to the bell shape of the DME/TACAN pulses. Their tails stretch below the noise floor, and thus cannot be removed by pulse blanking alone. In addition, when blanking the pulse interference, the E5 signal that coincides with the pulses is also blanked out. In this example, the DME/TACAN pulses occur 10–14 % of the time. Pulse blanking would thus blank out 10–14 % of the E5 signal, reducing its power. In the cases when the pulses are extremely dense in time, pulse blanking will blank out a

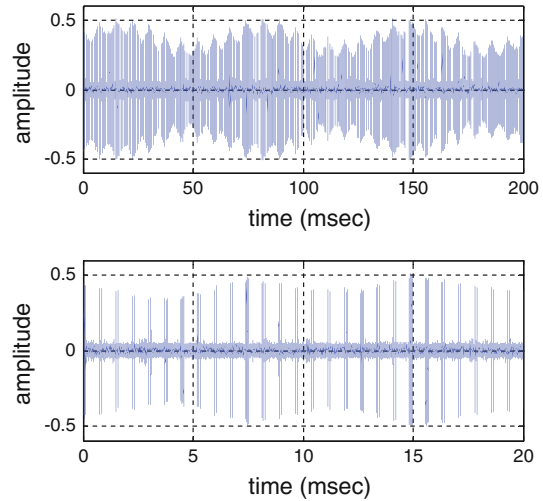


**Fig. 6** Received E5a signal. Inphase samples (top), zoom (bottom)

large portion of the GNSS signal or even the whole signal. It will make the signal unavailable and thus tracking will fail. In practice, the dynamics of the pulse blanker and the related recovery time are also an issue of time domain pulse blanking.

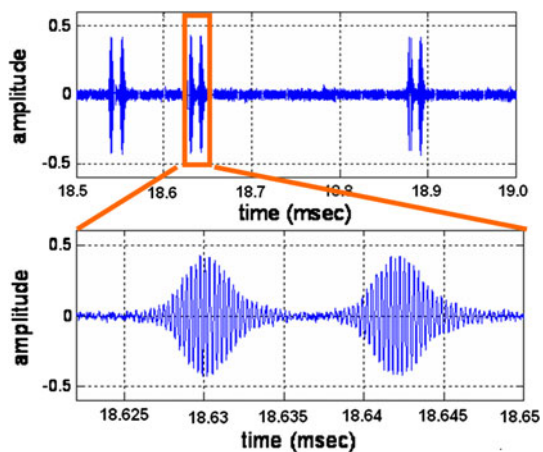


**Fig. 7** DME pulses are pairs of Gaussian pulses with pulse width of 3.5 μs and inter-pulse interval of 12 μs

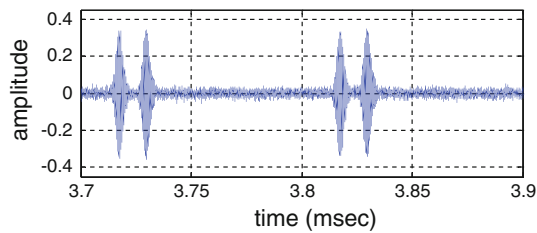


**Fig. 8** Time domain E5a signal before pulse blanking

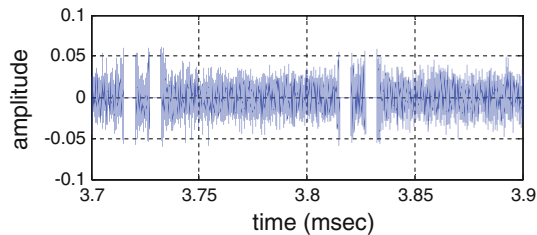


**Fig. 9** Time domain E5a signal after pulse blanking

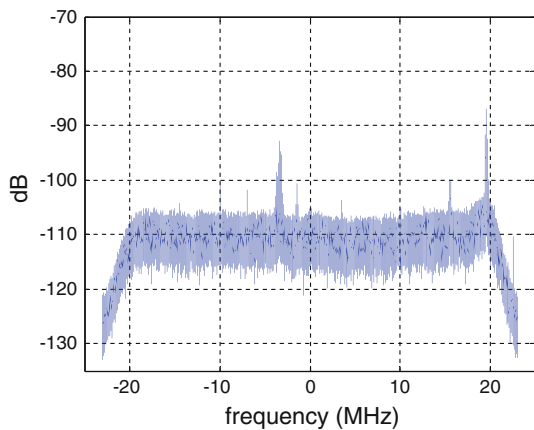


**Fig. 10** E5a power spectral density estimate, after pulse blanking

In addition to pulse blanking, there are other time domain approaches, which share the same drawbacks as pulse blanking. For example, a well-designed multi-bit A/D converter can suppress a constant envelope interference or pulsed interference if the quantizing levels are properly set (Amoroso 1983, 1986; Parkinson and Spilker 1996).

Existing frequency domain algorithm: notch filtering

The DME/TACAN signals have pulse characteristics not only in the time domain, but also in the frequency domain. In the frequency spectrum, the DME/TACAN signals appear as narrow-band frequency tones. Each frequency tone represents the signal from a nearby airport beacon. This motivates us to mitigate the DME/TACAN interference by notch filtering. Notch filtering removes the

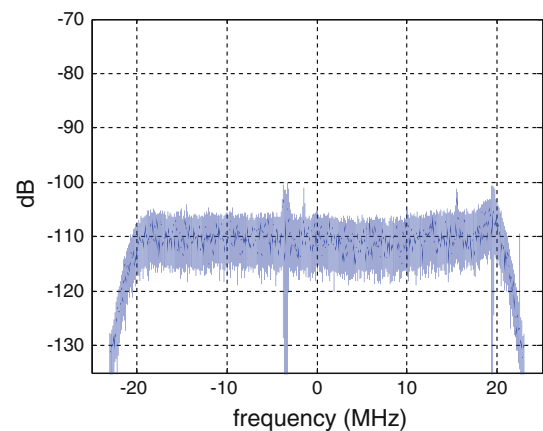


**Fig. 11** E5a power spectral density estimate, after notch filtering

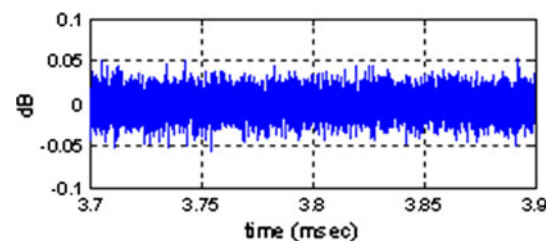


**Fig. 12** Time domain E5a signal, after notch filtering

frequency components that exceed a certain level of the noise spectral density as shown in Fig. 11. A variety of notch filters are discussed in (Wang and Milstein 1988; Krishnamurthy and Logothetis 1999; Symons 1978; Soderstrand and Johnson 1997, 2006).

Notch filtering has two advantages. First, it can completely suppress the DME/TACAN interference, including both the central part and the tails of the Gaussian pulses. As the DME/TACAN signals only occur at certain frequencies, if the signal power at these frequency components is filtered out, DME/TACAN interference can be eliminated. Second, compared to time domain pulse blanking, it preserves more of the energy of the E5 signal coincident with the interference pulses in the time domain. Figure 12 shows the notch filtered data from the same time period as in Fig. 8. The interference pulses disappear, while the E5 signal along with thermal noise remains.

However, notch filtering also has its drawbacks. Besides the interference, it also removes the E5 signal energy at the DME/TACAN frequencies. Since each nearby DME/TACAN beacon is mapped as a spike in the spectrum, a large number of beacons in the surrounding area will result in many spikes in the spectrum. When filtering the frequency components regarding to the spikes, a large portion of the GNSS signal will also be filtered out. Even during the time period when there are no DME/TACAN pulses, the E5 signal at these frequencies is still filtered. Moreover,

the design of the notch filter will become complicated as the number of nulls increases. The filter design is even more complicated for situations such as GPS receivers equipped on aircraft. The DME environment constantly changes as the aircraft flies over different transponders. This requires the airborne receiver to have a table of all nearby airports/DME transponders and their associated frequencies. The airborne receiver then has to change the notch filter accordingly as the airplane travels, which makes the notch filtering method impractical for non-stationary users.

#### Proposed algorithm: time–frequency hybrid blanking

Pulse blanking and notch filtering both have advantages and disadvantages. Pulse blanking only functions when pulse interference occurs, but it cannot eliminate the pulses completely. It also has the side effect of blanking the E5 signal superposed with the pulses. Notch filtering can suppress the pulse interference thoroughly and preserve most of the energy of the E5 signal energy coincident with the pulses, but it degrades the signal power even when there are no DME/TACAN pulses. The notch filter design becomes difficult when there are several notches in the filter due to the number of DME/TACAN transponders.

We propose another DME/TACAN interference mitigation technique, hybrid blanking, which combines the advantages of pulse blanking and notch filtering. The schematic of this technique is shown in Fig. 13 (Gao et al. 2007). First, the incoming signal is passed through a sliding window. The next step is time domain pulse detection. In the time domain, if the amplitude of the incoming complex signal exceeds a certain level of the noise floor, a DME/TACAN pulse is detected. The pulse position is then estimated based on the center of mass of the signal in the

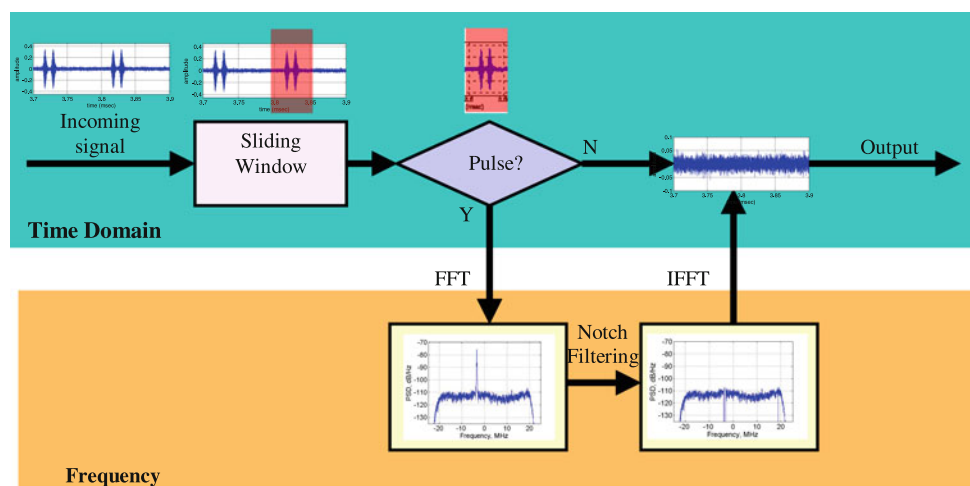
segment. The duration of the pulses is also estimated. The pulse detection and the pulse center estimation trigger notch filtering. The segment of data centered at the estimated pulse position with the estimated pulse duration is then converted into the frequency domain and is fed into a notch filter by blanking all FFT bins above a given threshold, which does not require to have a priori knowledge of nearby DME transponder frequencies. The filtered piece of data is then converted back to the time domain and replaces the original portion as the output.

Figure 14 shows the selectivity of the three mitigation techniques, pulse blanking, notch filtering, and hybrid blanking. Hybrid blanking is shown as the red dots. Hybrid blanking is only implemented when DME/TACAN pulses exist. It overcomes the disadvantage of regular notch filtering, which always suppresses the corresponding frequency components of the signal even when there is no interference. For the slices of the data that are covered by DME/TACAN pulses, hybrid blanking preserves most of the signal energy as shown in Figs. 15 and 16. This overcomes the disadvantage of time domain pulse blanking.

#### Hardware implementation trade-off: FDAF

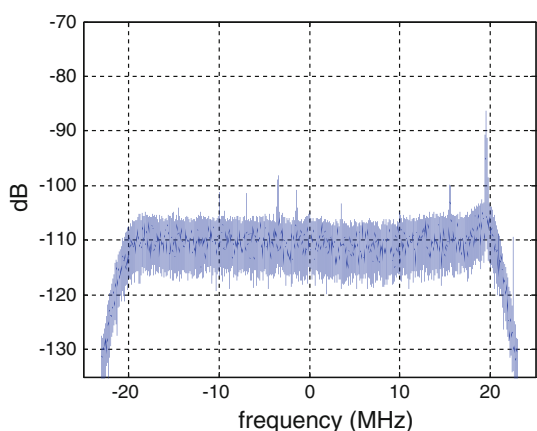
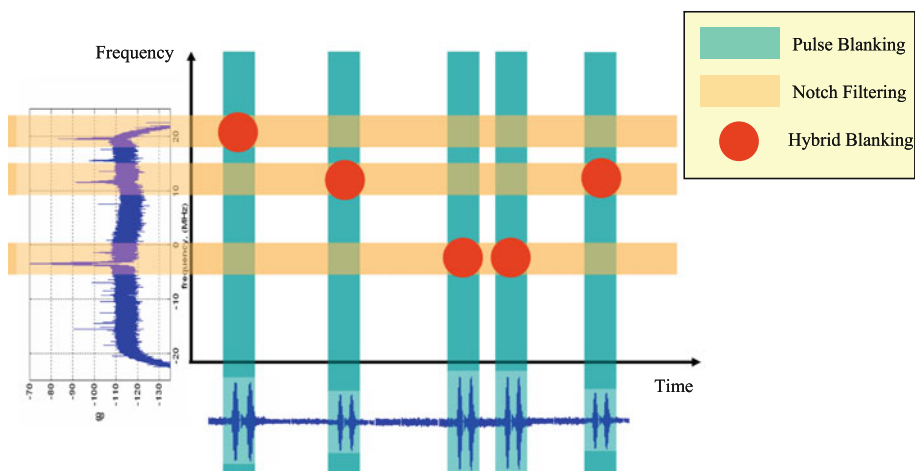
Hybrid blanking maximizes the remaining GNSS signal energy. When implementing in the hardware, we simplify the algorithm as a trade-off for complexity and performance. We name simplified hybrid blanking FDAF.

Figure 17 illustrates the difference between hybrid blanking and FDAF. Instead of detecting the pulse centers in time, we divide the time domain signal into a certain number of bins for FDAF. The bins containing the detected pulse pair center are further processed with notch filtering. The pulse pairs are not necessarily centered in the bins.



**Fig. 13** Hybrid blanking schematic

**Fig. 14** Selectivity of pulse blanking, notch filtering and hybrid blanking



**Fig. 15** E5a power spectral density estimate, after hybrid blanking. The signal has been down-converted to the baseband

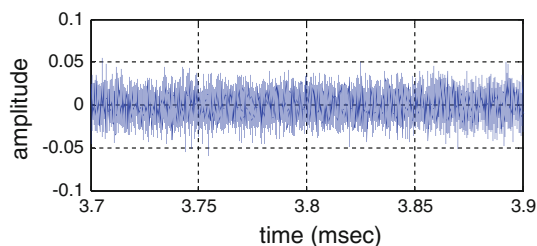


**Fig. 16** Time domain E5a signal, after hybrid blanking

Compared with hybrid blanking, FDAF is simpler to implement, because we no longer need to calculate and identify the locations of DME pulse series.

**On-flight data collection at European DME hotspot**

We test our DME mitigation techniques via data, which were collected within the frame of ANASTASIA (airborne new and advanced satellite techniques and technologies in

a system integrated approach). ANASTASIA was an integrated project funded by the European community’s sixth framework programme (DG research). The goal of ANASTASIA research was to provide on-board communication, navigation, and surveillance (CNS) solutions to cope with the expected increase in air traffic by 2020 (European Commission 2009).

Within the project ANASTASIA, a measurement campaign was carried out by DLR in March 2009 in order to obtain better and realistic data for the interference situation in the E5 band for aviation. For this purpose, flight trials were performed at different altitudes, and data were

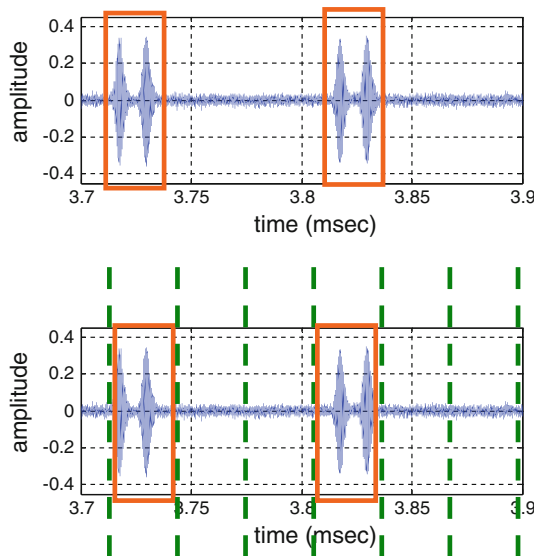


**Fig. 17** Illustration of the difference between hybrid blanking and FDAF. For hybrid blanking, the received signal segments are centered at the detected pulse pair center. These segments are then further processed with notch filtering (top). For FDAF, the received signal is first divided into evenly spaced bins. The bins containing the detected pulse pair center are further processed with notch filtering. The pulse pairs are not necessarily centered in the segments (bottom)

recorded with a GNSS E5/L1 antenna (Steingass et al. 2009). The data were already used for a test of a hardware receiver (Denks et al. 2009) following as close as possible the Galileo MOPS test procedures (EUROCAE 2007). We reuse this data to verify the effectiveness of our DME mitigation algorithms.

Figure 18 shows the test aircraft, a Dassault Falcon 20E which is owned by the German aerospace center DLR (Deutsches Zentrum für Luft- und Raumfahrt e.V.). This small jet is able to go to a maximum altitude of 42,000 ft (12,800 m). Figure 19 shows the skyward looking ANASTASIA navigation antenna mounted on top of the test aircraft. Most but not all of the interferers are radiating from the ground and, therefore, are not in the direct line-of-sight view of the antenna. Nevertheless, these reach the antenna by propagating along the aircraft body.

The main area of interest for the measurement campaign in a geographic sense was around Frankfurt/Main, Germany, where the European hotspot with respect to DME/TACAN is located (Fig. 20). The data used for this investigation belong to the “hotspot” position (coordinates: 50°3′N, 8°5′E) at the following altitudes:

- 1,473 m (4,800 ft) (FL50)
- 4,520 m (14,800 ft) (FL150)
- 8,833 m (29,000 ft) (FL 300)
- 11,155 m (36,600 ft) (FL 380)

The analyzed snapshots were carefully selected when the aircraft had a bank angle of zero degrees. This is important because during turns of the aircraft with non-zero banking angles line-of-sight connections between the interferers on the ground and the receiving antenna onboard could be established and thus result in higher power levels.

Figure 21 shows the equipment setup for the measurements during the flight trials. The received signal is first fed into a low-noise antenna preamplifier (LNA) and then enters the RF-frontend (FE), where filtering and additional amplification take place. The total RF-amplification is approximately 45 dB. For the main measurement equipment, a vector power spectrum analyzer (Agilent E4443A (PSA)) is used. The PSA executes the down conversion as



**Fig. 18** DLR’s Test aircraft: Dassault Falcon 20 E



**Fig. 19** ANASTASIA navigation antenna mounted on top of test aircraft



**Fig. 20** Test area “European hotspot” near Frankfurt/Germany

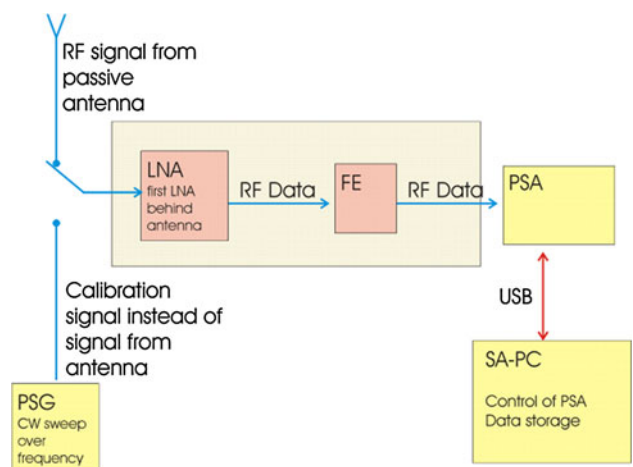


**Fig. 21** Test setup for data collection

well as the digitization with a bandwidth of up to 80 MHz. The control of the PSA is done via a personal computer (SA-PC). The data files containing the interference data are stored in that SA-PC. For calibration purpose, a signal



generator (PSG) is connected to the LNA instead of the passive antenna prior to every flight to obtain the characteristics of the measurement setup. These data are also collected by the PSA.

**Flight and ground test results**

Figures 22, 23, 24, and 25 show the power spectral density of the flight test data captured at different altitudes around Frankfurt, Germany. The spikes shown in the spectrum are DME/TACAN signals. At 1,473 m altitude, about ten DME/TACAN signals from the local ground transponders are shown in the frequency span of 80 MHz. As the altitude rises, more DME/TACAN signals are captured by the in-flight receiver. At an altitude of 11,155 m, the number of received DME/TACAN signals reaches the peak of more

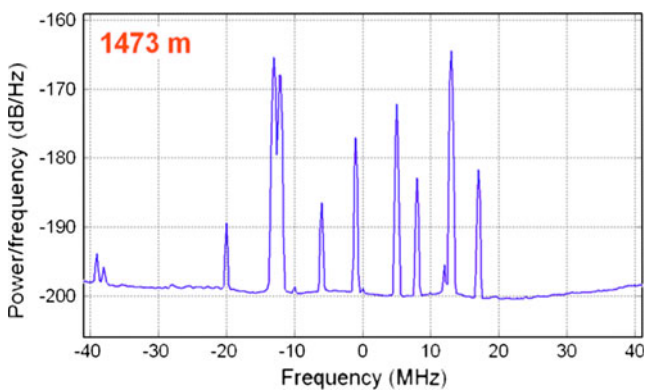


**Fig. 22** Frequency domain representation of flight test data measured at altitude of 1,473 m. The signal has been down-converted to the baseband. The pulses shown in the frequency domain are the DME/TACAN signals

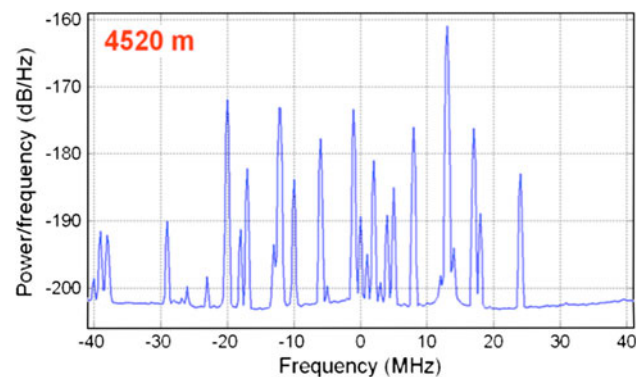


**Fig. 23** Frequency domain representation of flight test data measured at altitude of 4,520 m. The signal has been down-converted to the baseband. As the altitude rises, the number of received DME/TACAN signals also increases

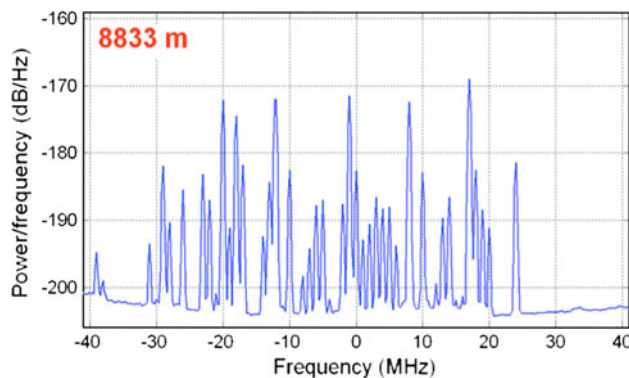


**Fig. 24** Frequency domain representation of flight test data measured at altitude of 8,833 m. The signal has been down-converted to the baseband

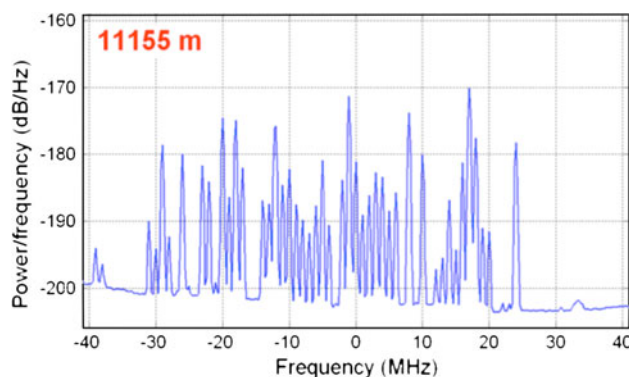


**Fig. 25** Frequency domain representation of flight test data measured at altitude of 11,155 m. The signal has been down-converted to the baseband. The number of received DME/TACAN pulses reaches the peak of more than 40

than 40. The reason is the following. At low altitude, some of the DME signals are blocked by geographic barriers, such as buildings or mountains. At high altitude, the receiver receives more line-of-sight signals due to fewer blockages.

To test our DME/TACAN algorithms, we synthesize our data set by adding the locally generated noise-free GPS PRN 25 L5 signal to the captured flight test data of the DME/TACAN environment. We also carefully calibrate the power of the generated GPS L5 signal based on the noise floor of the flight test data, so that its  $C/N_0$  after interference mitigation matches that of the live L5 data from our patch antenna. Note that the purpose of our experimental results is to compare the effectiveness among different interference mitigation techniques, so we focus on the relative  $C/N_0$  rather than the absolute values. Currently, the full constellation of satellites carrying either Galileo E5 or GPS L5 signals is not available. In fact, there are only a couple of satellites in both Galileo and GPS systems with

the E5/L5 payload. It is challenging to schedule the flight test so that there are GPS or Galileo satellites with L5 or E5 payload not only in view, but also at a desired elevation angle. Therefore, we believe our synthesized data set is the practical way of testing the performance of our mitigation algorithms.

We apply all mitigation algorithms mentioned in this paper to our data set, including pulse blanking, notch filter, our proposed hybrid blanking, and FDAF for implementation simplification. The pulse blanker applied assumes no latency in pulse detection and no recovery delay.

We use two sets of figure of merits to evaluate the algorithm performance. One set is based on the acquisition results. Specifically, these are correlation peak to next peak ratio (CPPR) and the correlation peak to mean peak ratio (CPPM). The next peak indicates the second strongest peak within one chip duration. In quiet situation, the main peak is dominant. However, in a noisy environment with high interference, the second peak can overpower the main peak, causing tracking loops locking to the wrong peak.

**Table 2** Tracking loop parameters of the software receiver used to test DME mitigation algorithms

Tracking loops	Bandwidth (Hz)
FLL	60
Non-coherent PLL	40
Intermediate coherent PLL	15
Steady-state coherent PLL	7

The other set is based on the tracking results, or the signal-to-noise ratio of the tracked GNSS signal. The carrier tracking loop starts in the frequency lock loop (FLL) mode for initial frequency pull-in, then transitions to a non-coherent phase lock loop (PLL) until there are enough navigation data bit transitions to determine the data bit boundary, then goes to an intermediate set of loop filter coefficients for a coherent PLL, and finally reaches the narrowest bandwidth PLL for steady-state tracking. The noise bandwidths of the tracking loops are listed in Table 2.

We compare among different DME/TACAN mitigation techniques, namely original data set with no mitigation algorithm, pulse blanking, notch filtering, hybrid blanking, and FDAF. For notch filtering, we have tested both cases for an FFT-based notch filter and a finite impulse response (FIR) notch filter. The FFT notch filter zeroes out all spikes in the frequency domain, whereas the FIR notch filter only attenuates up to 10 frequency bins. In comparison with the FFT notch filter, the FIR notch filter is a more practical notch filter in hardware. For FDAF, we tested both longer piecewise segments of 2.3 ms, and shorter piecewise segments of 13 μs. The comparison is for the worst DME/TACAN interference situation, which is at the European DME hotspot near Frankfurt, Germany, and at the altitude of 11,153 m with the maximum received DME/TACAN pulses as shown in Fig. 25.

Figures 26 and 27 show the comparison results. Our proposed hybrid filtering and FDAF outperform the traditional pulse blanking and notch filtering. For FDAF, the performance is dependent on the length of piecewise segments. When the piecewise segments are as long as 2.3 ms, the FDAF algorithm is only a little better than FFT-based

**Fig. 26** Performance comparison among different DME/TACAN mitigation techniques for the worst-case situation. The data set contains flight test data captured at European DME hotspot at 11,153 m altitude near Frankfurt, Germany. CPPR and CPPM are the figures of merits based on the receiver acquisition results

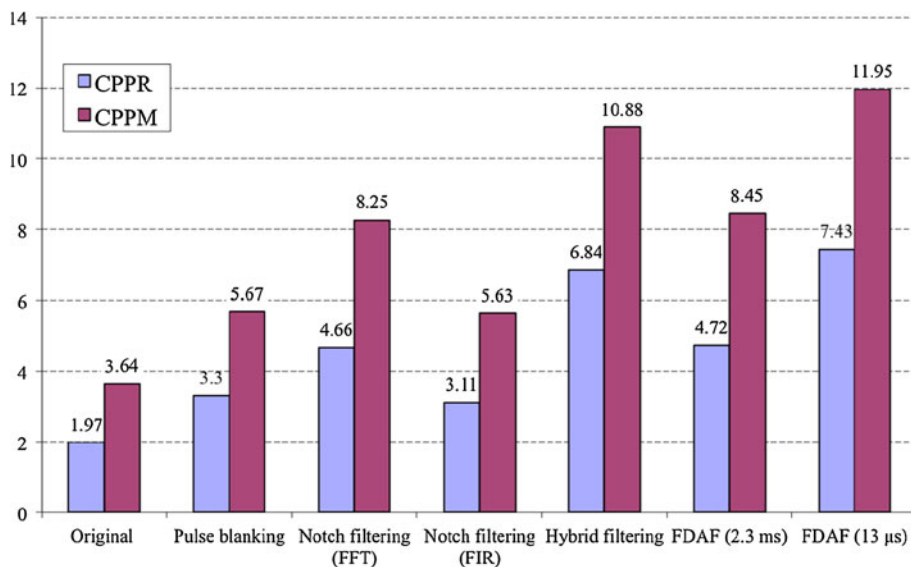


**Fig. 27** Performance comparison among different DME/TACAN mitigation techniques for flight test data captured at European DME hotspot at 11,153 m altitude near Frankfurt, Germany.  $C/N_0$  is the figure of merits based on the receiver tracking results

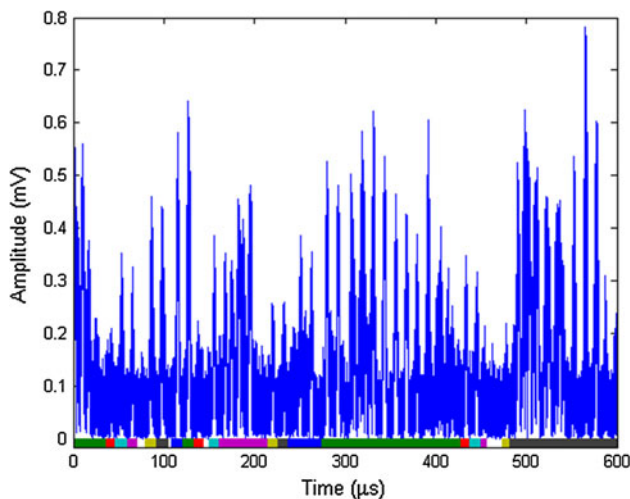
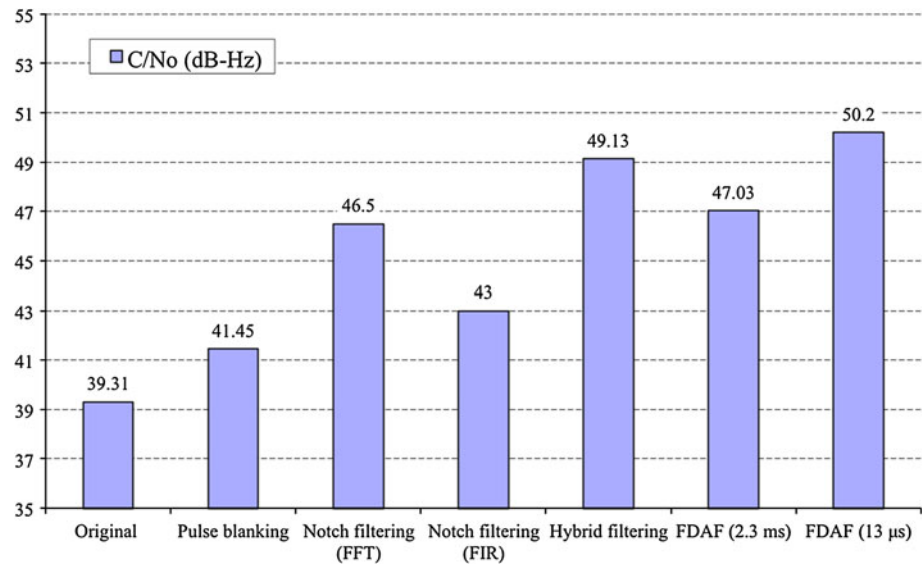


**Fig. 28** Time domain representation of the signal in Fig. 25. The colorful horizontal lines along the  $x$ -axis indicate the filtering windows implemented by our hybrid blanking algorithm. It is challenging to detect the correct pulse centers or determine appropriate filtering windows when the DME/TACAN pulses are so crowded

notch filtering. In particular, the  $C/N_0$  gain over FFT-based notch filtering is only 0.53 dB. However, when the piecewise segments are as short as 13  $\mu$ s (barely covers a DME/TACAN pulse pair), FDAF has even better performance than hybrid blanking. The reason is the following. For the worst-case situation, the DME/TACAN pulses in the time domain are crowded as shown in Fig. 28. In fact, the pulses are so crowded that they often overlap with each other and generate pulse clusters (Fig. 28). The colorful horizontal lines along the  $x$ -axis indicate the filtering windows implemented by our hybrid blanking algorithm. It is

challenging to detect the correct pulse centers or determine appropriate filtering windows.

For brevity, we do not show the results for the synthesized flight test data at other altitudes, because the data of 11,153 m elevation represent the worst-case situation of DME/TACAN interference.

In addition to the worst-case situation at the European DME hotspot, we also test our mitigation algorithms under a quieter situation, which is on the roof of our Stanford GPS Laboratory. The data are collected by a commercial patch antenna when PRN 25 L5 signal is in view.

Figures 29 and 30 show the performance comparison among different DME/TACAN mitigation techniques for a quieter-case situation at Stanford, CA, USA. This time, our hybrid blanking algorithm outperforms not only traditional pulse blanking and notch filtering, but also FDAF. There is not much performance difference for FDAF with different piecewise segment lengths. Figure 31 shows that for the quieter situation, the DME/TACAN pulses in the time domain are not as dense as shown in Fig. 28. Although the duty cycle of the DME pulses at Stanford is low, due to the high power of pulses, such low rate of pulses still cause about 9 dB of loss for a non-mitigated receiver. Our hybrid blanking algorithm well detects the correct pulse centers and determines appropriate filtering windows. Due to sparse pulses, there is not much difference for FDAF in terms of segment lengths.

## Conclusion

We described the DME/TACAN signals as interference to the GNSS signals by presenting both time and frequency

**Fig. 29** Performance comparison in terms of CPPR and CPPM among different DME/TACAN mitigation techniques for quieter situation. The data set is captured by a commercial patch antenna on the roof of our Stanford GPS Laboratory at Stanford, CA, USA

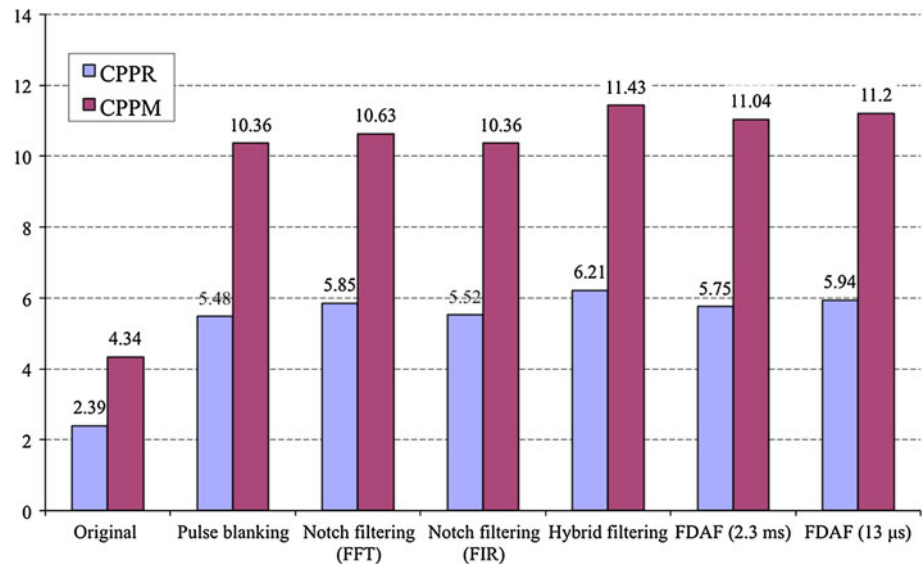
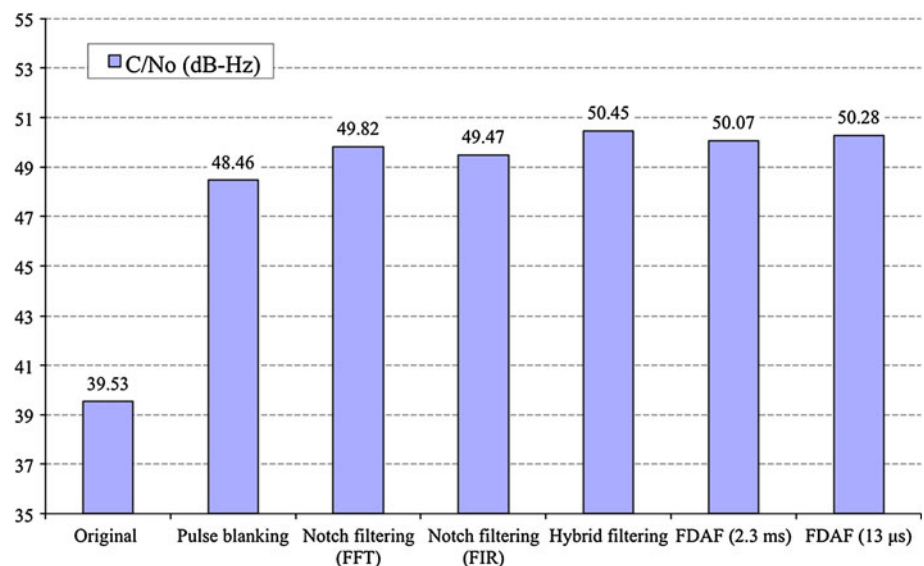


**Fig. 30** Performance comparison in terms of C/N0 among different DME/TACAN mitigation techniques for quiet situation. The data set is captured by a commercial patch antenna on the roof of our Stanford GPS Laboratory at Stanford, CA, USA



representations of the real received signals. In addition to the existing mitigation algorithms, such as pulse blanking and notch filtering, we proposed the time–frequency hybrid blanking algorithm and FDAF as a simplified version for hardware implementation.

In order to evaluate the performance of the above mitigation algorithms with a worst-case situation, we utilized data which were conducted in a flight campaign with a Falcon 20E aircraft over the European DME hotspot near Frankfurt, Germany. We also set up a commercial patch antenna at Stanford, CA, USA to test the quieter situation. We have applied the above mitigation algorithms to both

the worst- and quieter-case situations to evaluate their performance.

Our experimental results show that our proposed time–frequency hybrid blanking algorithm outperforms pulse blanking and notch filtering in both worst- and quieter-case situations. The simplified version, FDAF, is a sub-optimal solution and is more practical for hardware implementation. The performance of FDAF highly depends on the piecewise segment lengths when DME/TACAN pulses are clustered in time in the worst-case situation. However, for the quieter-case situation where the DME/TACAN pulses are sparse, such dependence on piecewise segment lengths is small.

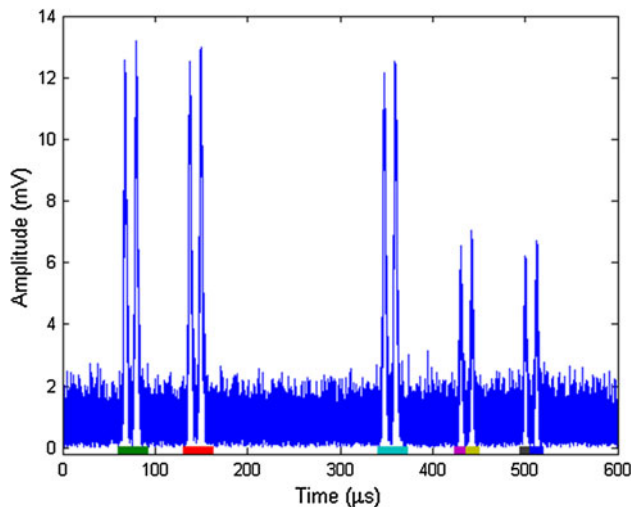


**Fig. 31** Time domain representation of the signal environment on the roof of our Stanford GPS Laboratory at Stanford, CA, USA. The colorful horizontal lines along the x-axis indicate the filtering windows determined by our hybrid blanking algorithm. The algorithm well detects the correct pulse centers and determines appropriate filtering windows, because when the DME/TACAN pulses are not as dense as these in Fig. 28

**Acknowledgments** This work was supported in part by the US Federal Aviation Administration under Grant—G-007 and by the European Commission.

## References

- Amoroso F (1983) Adaptive AID converter to suppress CW interference in DSPN spread-spectrum communications, *IEEE Trans Commun, Com-31*(10)
- Amoroso F (1986) Performance of the adaptive A/D converter in combined CW and gaussian interference, *IEEE Trans Commun, Com-34*(3)
- Bastide F, Chatre E, Macabiau C, Roturier B (2004) GPS L5 and galileo E5a/E5b signal-to-noise density ratio degradation due to DME/TACAN signals: simulation and theoretical derivation. ION NTM Conference, San Diego, CA
- Denks H, Hornbostel A, Perré J-M (2008) GNSS receiver testing focusing on strong interference by use of a hardware signal simulator, In: *Proceedings of ION 08, Savannah GA*
- Denks H, Hornbostel A, Chopard V (2009) GNSS receiver testing by hardware simulation in a standardized pulsed and CW interference environment. In: *Proceedings of ENC GNSS, Naples, 2009*
- EUROCAE (1987) Minimum operational performances requirements for distance measuring equipment (DME/N and DME/P) Interrogators Operating Within the RF Range 960 to 1215 MHz (airborne equipment) EUROCAE ED-84
- EUROCAE (2007) Interim minimum operational performance specification for airborne Galileo satellite receiving equipment, vs. 0.25
- European Commission (2009) [www.anastasia-fp6.org](http://www.anastasia-fp6.org)
- Gao GX (2007) DME/TACAN interference and its mitigation in L5/E5 bands, ION global navigation satellite systems conference 2007. Fort Worth, Texas
- Gao GX, De Lorenzo D, Chen A, Lo S, Akos D, Walter T, Enge P (2007) Galileo GIOVE-A broadcast E5 codes and their application to acquisition and tracking. ION NTM Conference, San Diego, CA
- Kayton M, Fried W (1997) *Avionics navigation systems*, 2nd edn. Wiley, New York
- Kim T, Grabowski J (2003) Validation of GPS L5 Coexistence with DME/TACAN and Link-16 System ION GNSS conference, Portland, OR
- Krishnamurthy V, Logothetis A (1999) Adaptive nonlinear filters for narrow-band interference suppression in spread-spectrum CDMA systems, *IEEE Trans Commun, 47*(5)
- Parkinson B, Spilker JJ (1996) *global positioning system: theory and applications*, vol I, AIAA, 1st edn
- RTCA DO-292 (2004) Assessment of radio frequency interference relevant to the GNSS L5/E5A frequency band
- Soderstrand, M, Johnson, TG, Strandberg RH, Loomis HH, Rangarao KV (1997) Suppression of multiple narrow-band interference using real-time adaptive notch filters, *IEEE Trans Circuits Syst II: Analog and Digit Signal Process, 44*(3)
- Soderstrand M, Johnson L, Phillips S, Steven R (2006) New technique for attenuation of narrow-band interference with applications in control and communications systems. Fortieth Asilomar Conference on Signals, Systems and Computers
- Steingass A, Hornbostel A, Denks H (2009) Airborne measurements of DME interferers at the European hotspot, In: *Proceedings of ENC GNSS, Naples*
- Symons F (1978) Narrow-band interference rejection using the complex linear prediction filter', *IEEE Trans Acoust Speech Signal Process, 26*(1)
- Wang Y-C, Milstein LB (1988) Rejection of multiple narrow-band interference in both BPSK and QPSK DS spread-spectrum systems, *IEEE Trans Commun, 36*(2)

## Author Biographies

**Grace Xingxin Gao** is an assistant professor in the Aerospace Engineering Department at University of Illinois at Urbana-Champaign. She obtained her PhD from Stanford University in 2008. She was a research associate at Stanford University from 2008 to 2012.

**Liang Heng** is a postdoctoral researcher in the Aerospace Engineering Department at University of Illinois at Urbana-Champaign. He obtained his PhD in Electrical Engineering from Stanford University in 2012.

**Achim Hornbostel** is a research associate at the Institute of Communications and Navigation at the German Aerospace Center (DLR). His main activities are currently in signal propagation, hardware simulation, and receiver development. He is member of ION, EUROCAE WG62, and VDE/ITG section 7.5 “Wave Propagation.”

**Holmer Denks** is an In Orbit Testing (IOT) Engineer with DLR-GfR which is a private company who operates the Galileo Control Centre in Germany. Until January 2010, he was a research associate in the German Aerospace Center (DLR), where he worked on receiver algorithms and receiver testing.

**Michael Meurer** is the head of the Department of Navigation of the German Aerospace Center (DLR), Institute for Communications and Navigation, and the coordinating director of the DLR Center of Excellence for Satellite Navigation. His current research interests include GNSS signals, GNSS receivers, interference mitigation, and navigation for safety-critical applications.

**Todd Walter** is a senior research Engineer in the Department of Aeronautics and Astronautics at Stanford University. He is president of the Institute of Navigation where he is also a fellow and has received the Kepler and Thurlow Awards.

**Per Enge** is a professor of Aeronautics and Astronautics at Stanford University. He directs the GPS Research Laboratory.